HHS Public Access

Author manuscript

Radiat Res. Author manuscript; available in PMC 2023 October 05.

Published in final edited form as:

Radiat Res. 2023 September 01; 200(3): 223–231. doi:10.1667/RADE-23-00057.

Comparison of Tumor Control and Skin Damage in a Mouse Model after Ultra-High Dose Rate Irradiation and Conventional Irradiation

Kayla E. A. Duval[a,1], **Ethan Aulwes**[a,1], **Rongxiao Zhang**[a,b,c], **Mahbubur Rahman**[b], **M. Ramish Ashraf**[b], **Austin Sloop**[b,2], **Jacob Sunnerberg**[b,2], **Benjamin B. Williams**[a,b,c], **Xu Cao**[b], **Petr Bruza**[b], **Alireza Kheirollah**[a], **Armin Tavakkoli**[a], **Lesley A. Jarvis**[a,c], **Philip E. Schaner**[a,c], **Harold M. Swartz**[a], **David J. Gladstone**[a,b,c], **Brian W. Pogue**[a,b,c,d], **P. Jack Hoopes**[a,b,c,3]

[a]Geisel School of Medicine, Dartmouth College, Hanover, New Hampshire

[b]Thayer School of Engineering, Dartmouth College, Hanover, New Hampshire

[c]Dartmouth Cancer Center, Dartmouth-Hitchcock Medical Center, Lebanon, New Hampshire

[d]Department of Medical Physics, University of Wisconsin, Madison, Wisconsin

Abstract

Recent studies suggest ultra-high dose rate radiation treatment (UHDR-RT) reduces normal tissue damage compared to conventional radiation treatment (CONV-RT) at the same dose. In this study, we compared first, the kinetics and degree of skin damage in wild-type C57Bl/6 mice, and second, tumor treatment efficacy in GL261 and B16F10 dermal tumor models, at the same UHDR-RT and CONV-RT doses. Flank skin of wild-type mice received UHDR-RT or CONV-RT at 25 Gy and 30 Gy. Normal skin damage was tracked by clinical observation to determine the time to moist desquamation, an endpoint which was verified by histopathology. Tumors were inoculated on the right flank of the mice, then received UHDR-RT or CONV-RT at 1 × 11 Gy, 1 × 15, 1 × 25, 3 × 6 and 3 × 8 Gy, and time to tumor tripling volume was determined. Tumors also received 1 × 11, 1 × 15, 3 × 6 and 3 × 8 Gy doses for assessment of CD8+/CD4+ tumor infiltrate and genetic expression 96 h postirradiation. All irradiations of the mouse tumor or flank skin were performed with megavoltage electron beams (10 MeV, 270 Gy/s for UHDR-RT and 9 MeV, 0.12 Gy/s for CONV-RT) delivered via a clinical linear accelerator. Tumor control was statistically equal for similar doses of UHDR-RT and CONV-RT in B16F10 and GL261 murine tumors. There were variable qualitative differences in genetic expression of immune and cell damage-associated pathways between UHDR and CONV irradiated B16F10 tumors. Compared to CONV-RT, UHDR-RT resulted in an increased latent period to skin desquamation after a single 25 Gy dose (7 days longer). Time to moist skin desquamation did not significantly differ between UHDR-RT and CONV-RT after a 30 Gy dose. The histomorphological characteristics of skin damage were similar for UHDR-RT and CONV-RT. These studies demonstrated similar tumor control responses for equivalent single and fractionated radiation doses, with variable difference

[3] Corresponding author's P.Jack.Hoopes@dartmouth.edu.

[1]These authors contributed equally to this study.

[2]Scholar in Training.

in expression of tumor progression and immune related gene pathways. There was a modest UHDR-RT skin sparing effect after a 1 × 25 Gy dose but not after a 1 × 30 Gy dose.

INTRODUCTION

Although radiation treatment (RT) has been a staple of cancer treatment for over a century, normal tissue damage (both early and late) is the primary radiation dose and cure-limiting factor. Additionally, tumor type, location, volume, and intrinsic radiosensitivity all factor into the ability of radiation to achieve robust cancer control. Achieving an improved radiation therapeutic ratio is based on increased tumor radiosensitivity and /or decreased normal tissue radioresistance. Conventional dose fractionation schemes attempt to strike an optimal balance between tumor control and normal tissue health; as such, it is common practice to use many small doses over 6–7 weeks (e.g., 35 fractions of 2 Gy). However, there has been a recent shift towards application of hypofractionated radiotherapy (larger and fewer radiation fractions) in both the definitive and palliative therapy setting (1–3). Despite anticipated improved tumor control, there is still caution regarding the potential for unknown detrimental late effects from unconventional radiation therapy regimens.

Recently, ultra-high dose rate (UHDR) radiation therapy has shown the ability to spare normal tissue, in what has been called the FLASH effect, as compared to conventional dose rate (CONV) radiation therapy, without compromising tumor control (4). Although the use of UHDR treatment in rodent studies was first reported in the 1970s and 1980s, the information is limited and not highly comparable to more recent studies (5–7). At present, specialized linear accelerators (electrons), clinical proton accelerators, and kV X-ray systems have been successfully converted and used for UHDR studies. A comprehensive assessment of comparable UHDR- and CONV-treated rodent tumors showed an essentially equal number of studies in which UHDR-RT was more effective, CONV-RT was the more effective, or there was no difference (8). Importantly, the differences when present, were modest. A recent study from Liljedahl et al., in a rat glioblastoma model (subcutaneous and intracranial tumors), demonstrated little difference in tumor control, and selected apoptosis, cytotoxic and immune pathways, after comparable UHDR-RT and CONV-RT (9). Most normal tissue studies were conducted in mouse skin, lung, and/or brain tissue, and most showed reduced skin toxicity in UHDR-RT mice compared to CONV-RT at doses ranging from 10–48 Gy (10–15). One study showed a several-month delay or absence of ulceration at doses of 30 Gy and 40 Gy (10). Vozenin et al. published a long-term pig skin toxicity study, which also showed reduced radiation damage after UHDR at a dose rate of 300 Gy/s and doses of 22 to 34 Gy (13). Although the key pathophysiology, temporal, and mechanistic aspects of the UHDR effect remain unclear, there are interesting hypotheses suggesting ultra-short radiation delivery time exposes/damages fewer circulating immune cells, thus limiting postirradiation lymphocyte loss, a reduction in DNA-damaging free radical biology, and the possibility that cell death pathway signaling may be affected. (12, 16).

The aims of this study were twofold. Using a murine flank skin tumor model, we compared tumor control and normal tissue damage after identical UHDR and CONV doses.

Tumor response to UHDR and CONV treatments was evaluated by genetic assessment, immunohistochemistry (IHC) staining for immune infiltration, and tumor growth kinetics. While there are many defined stages of radiation-induced skin damage, we modified a clinical dermatopathology grading system to address the current situation easily and accurately. The primary endpoint for normal tissue toxicity was the postirradiation time to moist desquamation/ulceration of skin after 25 Gy or 30 Gy. We then validated these clinical endpoints histologically, using conventional radiation pathology descriptions (17, 18).

Although radiation-induced skin damage is not often considered life-threatening, it can have a significant impact on patient quality of life in both the acute and late setting, and can compromise a patient's ability to complete the prescribed course of radiotherapy (19, 20). Therefore, any technique that spares radiation-induced skin damage (or other normal tissue damage), without compromising tumor control, has the potential to improve the radiation therapeutic ratio and a chance for cure.

METHODS

Cell Lines

In these studies, murine melanoma (B16F10) and murine glioma (GL261) cells were cultured and inoculated into the dermis of flank skin. B16F10 murine melanoma cells were cultured in RPMI media with 10% FBS and 1% antibiotics (penicillin – streptomycin, HyClone). GL261 murine glioblastoma cells were cultured in DMEM media with 10% FBS and 1% antibiotics. Both cell lines were incubated at 37°C and 5% CO_2.

Radiation Treatment

CONV and UHDR treatments were delivered on the same day, with a Varian Clinac 2100 C/D linear accelerator (linac) operating in normal clinical mode or in the converted UHDR mode. The linac used for these treatments was the same clinical machine on which Rahman et al. (21) demonstrated a reversible method of conversion to UHDR electron delivery with precise dose rates on the order of 270 Gy/s at treatment isocenter. For CONV treatment, a 9 MeV beam was used and for UHDR treatment a 10 MeV beam. Each animal was treated with either CONV or UHDR exposure, applied to the flank tumor or the normal skin (Fig. 1). Both irradiation methods used a circular cutout (ø = 18 mm) in combination with the 6 × 6 cm applicator to collimate the field (Table 1). The field was sufficient to cover each tumor with an approximate 2 mm peritumoral region. All tumor and normal doses (Tables 2 and 3) were verified with in vivo radiochromic film (Gafchromic Film), and CONV treatments were matched to the measured UHDR treatments. Film dosimetry, using calibration curves relating optical density to dose, as well as pulse delivery control, were performed using the same methods as Rahman et. al (21). The prescribed doses corresponded to 80% in percentage depth-dose (PDD) values in water.

All mice were maintained at a surgical anesthetic plane for all irradiation procedures. Anesthesia consisted of isoflurane (5% induction, 2.5% maintenance) in 100% oxygen. For the irradiation procedure, mice were immobilized with the irradiated leg supported underneath to achieve a uniform flat field. The treatment region was aligned to the isocenter

using a light field. A 5-mm bolus was placed on the skin or tumor surfaces to achieve maximum dose at the superficial dermis or tumor parenchyma. Table 1 summarizes the beam configuration used for tumor and normal skin irradiation.

Mouse Tumor Irradiation Model

Female and male 6–8-week-old C57BL6 mice purchased from the Jackson laboratory (Bar Harbor, ME) were used in all experiments. Mice were randomly divided between CONV, UHDR, and the B16F10 and GL261 tumor groups. Control groups were implanted with B16F10 and GL261 tumors but were not irradiated. Tumors were inoculated intradermally with 1.5×10^6 cells in the right flank skin (Fig. 1). Tumors were measured daily, in three dimensions, using calipers, with volume calculated as length × width × depth × pi/6 per the common ellipsoidal geometric tumor model. Due to different growth rates, B16F10 tumors were treated on post-inoculation day 8, and GL261 tumors were treated on day 11. At the time of treatment, B16F10 and GL261 tumors averaged 163 mm^3 (SEM = 31.2) and 103 mm^3 (SEM = 12.6), respectively. The irradiated mice were assigned to either the genetic/IHC analysis cohort or the tumor control cohort, as shown in Table 2. All animal studies were reviewed and approved by the Dartmouth College Institutional Animal Care and Use Committee (IACUC).

Tumors treated for genetic and IHC analysis received: 1 × 11, 1 × 15, 3 × 6, or 3 × 8 Gy. The dose schemes 1 × 11 Gy and 3 × 6 Gy have common use in published mouse experiments and similar BED values, as do 1 × 15 Gy and 3 × 8 Gy (22). The 1 × 25 Gy dose group was assessed for tumor control, but not for genetic or IHC analysis.

Genetic Expression

A select group of B16 tumors, received 1 × 11, 1 × 15, 3 × 6 or 3 × 8 Gy, were harvested 96 h postirradiation for mRNA-based (Nanostring Technologies) genetic assessment and CD8+/CD4− immunohistochemistry. RNA isolation and purification was performed immediately after euthanasia using the Qiagen RNeasy Mini Kit. mRNA expression was quantified via the NanoString PanCancer IO 360 (murine) panel. This panel quantifies the expression of 600 genes involved in 28 cancer-related cellular pathways, including tumor growth, tumor microenvironment, and immune response. Expression values were analyzed with the Nanostring nSolver Analysis software (v. 4.0) and Advanced Analysis Software (v. 2.0).

CD8+ and CD4+ Infiltration

Immunohistochemistry samples taken from 1 × 11, 1 × 15, 3 × 6, and 3 × 8 Gy irradiated tumors (n = 5 for each group), 96 h postirradiation, were stained for CD8+ and CD4+ positive T-cells. Standard immunohistochemistry staining techniques were used. For each cell type, 100 counts in 20 randomly chosen fields (2,000 counts), was performed. The average fraction of positive cells, compared to total cell number, was calculated, providing a relative percentage of each cell type in each radiation group.

Tumor Treatment Efficacy

Tumor control was defined by the after-treatment time required to achieve a threefold increase in tumor volume (tumor tripling time). Tumors were measured daily, in three dimensions, using calipers, with volume calculated as length × width × depth × pi/6. (common ellipsoidal geometric tumor model).

Normal Skin Irradiation Model

After hair removal, the left flanks of male and female C57/Bl6 mice received either UHDR or CONV treatments through an 18-mm-diameter circular region (Fig. 1). Treatments consisted of a single dose of 25 Gy or 30 Gy at 9 MeV (CONV) or 10 MeV (UHDR), as listed in Table 3.

To characterize the clinical changes in skin accurately and consistently, we developed a 4-point grading system to quantify the extent of damage (Table 4). This grading system encompasses dermatopathology changes from normal (healthy) skin to full thickness epidermal necrosis. The visible onset and occurrence of significant epidermal damage (loss of viability and integrity) is pathologically represented by the presence of non-viable epithelium and/or full thickness epidermal necrosis. Regular photographic documentation was performed on all animals to create a visual record of the progression and outcome of radiation-induced changes. Based on our 4-point grading system, we took our normal skin damage endpoint to be the length of time (days) from irradiation to the day that a given lesion reached a grade of 2 or greater.

Skin was assessed daily by multiple observers. Visual criteria for dry desquamation morphology included epidermal/keratin flaking and graying. Moist desquamation/ulceration consisted of the loss of viable epidermis and a yellow, serum-like coating of the underlying dermis.

Although it was not used as an endpoint, histological verification was performed on irradiated skin samples. All samples underwent immersion-fixation of in 4% neutral buffered formaldehyde and processing for routine histopathology. Samples were cut at 4 um thickness in a standard skin perpendicular presentation plane and stained with hematoxylin and eosin (H&E).

Statistical Methods

Using tumor control or normal tissue damage parameters, Kaplan Meier curves were constructed in Graphpad Prism. A log rank test was performed to determine statistically significant differences in time to endpoint. Multiple t-test comparison was conducted on Graphpad Prism to compare CD8+/CD4+ IHC count data for equivalent UHDR and CONV doses. Statistical significance was defined as $P < 0.05$.

Genetic data was analyzed by Rosalind® (https://rosalind.bio/), with a HyperScale architecture developed by Rosalind, Inc. (San Diego, CA). Normalization, fold changes and P values were calculated using criteria provided by Nanostring. Rosalind® follows the nCounter® Advanced Analysis protocol of dividing counts within a lane by the geometric mean of the normalizer probes from the same lane. Housekeeping probes to be used

for normalization are selected based on the geNorm algorithm as implemented in the NormqPCR R library (23). Abundance of various cell populations is calculated on Rosalind using the Nanostring Cell Type Profiling Module. Rosalind performs a filtering of cell type profiling results to include results that have scores with a P value greater than or equal to 0.05. Fold changes and P values are calculated using the fast method as described in the nCounter® Advanced Analysis 2.0 User Manual. P value adjustment is performed using the Benjamini-Hochberg method of estimating false discovery rates (FDR).

We identified significant individual gene and aggregated pathway expression levels for comparing UHDR to CONV treatments, as well as for comparing irradiated tumors to controls. Rosalind®'s analysis calculated log fold expression changes and P values for each gene and reported those which were above ±1.5 $\log_2$ fold change with $P < 0.05$. For aggregate pathway expression, two types of significance scores were calculated in Rosalind: undirected and directed global significance analysis (GSA) scores. According to the nCounter® user manual, GSA scores are computed by the root mean square of the t statistic for each gene within a given pathway; these scores (by definition) do not show direction of gene expression, but rather the size of overall gene expression differences, and are calculated using the equation below:

$$global\ significance\ score = \sqrt{\left(\frac{1}{p}\sum_{i=1}^{p} t_i^2\right)},$$

where p is the number of pathways and t_i is the t-statistic from the ith pathway gene.

Directed significance scores summarize overall up or down regulation across the genes in a pathway. The pathways with highest significance scores were qualitatively assessed.

Hypergeometric distribution was used to analyze the enrichment of pathways, gene ontology, domain structure, and other ontologies. The topGO R library (24), was used to determine local similarities and dependencies between GO terms in order to perform Elim pruning correction. Several database sources were referenced for enrichment analysis, including Interpro (25), NCBI (26), MSigDB (27, 28), REACTOME (29), and WikiPathways (30). Enrichment was calculated relative to a set of background genes relevant for the experiment.

RESULTS

mRNA Assessment of Irradiated B16F10 Tumors

Irradiated B16F10 tumors were assayed for genetic (RNA) expression via the Nanostring pan cancer panel at 96 h postirradiation. Differences in gene expression levels between UHDR and CONV treatments, at equal doses (1 × 15 Gy, 1 × 11 Gy, 3 × 6 Gy, 3 × 8 Gy), were calculated in Rosalind for each gene and the aggregated pathways. Qualitative review of the pathway-level expression data revealed the following trends:

1. UHDR and CONV treated tumors showed consistently higher expression of all 28 pathways compared to nonirradiated tumors, including acute phase inflammation pathways, such as mast cell function and toll-like-receptors (TLR).
2. The four dose groups did not demonstrate consistent pathway-level expression differences between UHDR and CONV treatments across the 28 tested pathways (Table 5).
3. UHDR treatment demonstrated comparatively high gene-level changes in expression of proteins involved in angiogenesis and vessel maintenance.

IHC Assessment of Irradiated B16F10 Tumors

Quantification of CD8+ and CD4+ cell numbers in 20 10× magnification fields per tumor demonstrated no difference between UHDR and CONV treatments in any of the dose groups except for the 1 × 11 Gy dose group. This change was only observed in CD8+ cells (Fig. 2).

Tumor Control

At the time of irradiation, B16F10 tumors were 163 mm^3 (SEM = 31.2) and GL261 tumors were 103 mm^3 (SEM = 12.6). All CONV doses were matched to measured UHDR doses. CONV doses had a potential error of ±0.3 Gy, and UHDR doses had a potential error of ±0.7 Gy. After 1 × 25 Gy there was no statistical difference in postirradiation tumor growth kinetics for either radiation type or tumor type, as measured by tumor tripling time (Fig. 3, Table 6). Five UHDR- and five CONV-irradiated tumors (GL261, 1 × 25 Gy) did not reach the 3× regrowth metric by day 47 postirradiation. These tumors are reflected as “cures” in the Kaplan Meier curves. Tumor tripling time for each tumor type, prescribed radiation type, and dose is shown in Fig. 3.

Irradiation of Normal Skin

The postirradiation dermatopathology findings for this study included dry desquamation and moist desquamation/ulceration, as described in the Methods section (Table 4). However, due to challenges in accurately identifying dry desquamation, we determined use of a single moist desquamation/ulceration endpoint (grade 2/3) to be the most accurate and easy to determine. Therefore, all data demonstrated in the postirradiation time to lesion Kaplan-Meier curves (Fig. 4e) are based on the 2/3 grade endpoint.

UHDR and CONV treatments were matched in terms of delivery and dose. The most significant differences were found in the prolonged onset of moist desquamation after UHDR irradiation at 1 × 25 Gy (Fig. 4e). After a 1 × 30 Gy dose, there was no significant difference ($P > 0.05$) in time to moist desquamation/ulceration (grade of 2/3) (Fig. 4e). The mean days on study for males and females were comparable (Table 7).

DISCUSSION

UHDR research has demonstrated possible modest, but potentially very important, normal tissue sparing without similar sparing in tumor tissues. If confirmed, we predict that this situation will be one of the most important therapeutic ratio enhancements in the past 50+

years. It appears UHDR treatment is now entering a second phase of physics/engineering and in vivo research. So far, UHDR physics and engineering studies have dominated the literature and have been responsible much of the notable success. However even this success is now being challenged by new radiation beam structure parameters, such as high dose per pulse (possibly as high as 10–15 Gy/pulse), that present new and even greater challenges. Some UHDR researchers now believe the "FLASH effect" cannot be fully achieved without such high dose/pulse parameters. Most in vivo studies have, to date, been rodent studies, and most of these comparative studies have demonstrated some level of UHDR normal tissue sparing and equal tumor control (8–10, 14, 30). However, several large animal studies, generally pigs and companion animals, have and are being conducted. Although results of large animal studies are too limited to summarize and quantify effectively, some studies have demonstrated translational FLASH effect normal tissue sparing, while others have not. All of this said, the pathophysiology and mechanism of the UHDR FLASH effect is not understood, especially in the context of dose fraction, total dose, and beam structure. Therefore, the second phase of animal studies should center on the adoption and use of the most effective beam parameters based on current information, i.e., total dose, fractionation and dose /pulse. In this study, we assessed treatment efficacy and genetic and immune cell responses in UHDR- and CONV-irradiated tumors (single and fractionated doses) and clinical dermatopathology endpoints in normal skin at 1 × 25 and 1 × 30 Gy (UHDR and CONV).

Tumor genetics/immunology.

As detailed in the Methods section tumors were assayed for genetic (RNA) expression, via the Nanostring pan cancer panel and for the infiltration of CD8+ and CD4+ at 96 h postirradiation. In summary, none of the four dose groups studies demonstrate consistent, statistically significant pathway-level expression differences between UHDR treatments and CONV treatments across the 28 tested cancer immune and cell death pathways. Although in-depth individual gene and pathway analysis is beyond the scope of this manuscript, it is appropriate to note that there was significant variation in the direction and magnitude of overall gene expression change, for some pathways, when comparing UHDR- to CONV treatments at the doses and dose regimens used. Ongoing analyses are focused on defining data which suggest that genetic expression changes, after UHDR irradiation, have (in an overall sense) greater variation compared to CONV irradiation. Additional ongoing analyses suggest gene-level changes in the expression of proteins involved in angiogenesis and vessel maintenance are significantly different for UHDR and CONV treatments. Histomorphometric assessment of the infiltration of CD8+ and CD4+ T-cells in the parenchyma of B16F10 tumors, 96 h postirradiation, showed only minor differences for UHDR treatment and CONV treatment; there was an exception at 1 × 11 Gy, where UHDR treatment had a significant comparative increased in CD81 cells. It is important to note that this change did not translate to improved tumor control at 1 × 11 Gy.

Tumor control.

Using two immunocompetent flank tumor models, with different radiosensitivities, we demonstrated similar tumor control metrics for UHDR and CONV at 4 dose/fraction levels (1 × 11, 1 × 15, 3 × 6 and 3 × 8 Gy). As mentioned previously, the 1 × 11 and 3 × 6 Gy

dose regimens and 1 × 15 and 3 × 8 Gy dose regimens had similar BED levels. With the possible exception of 1 × 15 Gy, tumor control was similar for UHDR and CONV at these doses and fractionation regimens. The 1 × 15 Gy UHDR treatment arm, which showed a significant improvement in tumor control, is challenged by an outlier making it difficult to make accurate comparisons. We acknowledge that the findings in this study were limited to subcutaneous implanted tumors (B16F10 melanoma and GL261 glioma) irradiated within a 1.8-cm field. In general, however, our findings closely match those of many other UHDR/CONV rodent tumor treatment comparisons. These include the recent Böhlen et al. (8) review of 66 studies comparing UHDR to CONV and the recently published UHDR vs. CONV response comparison in a rat glioblastoma tumor (9), which supported an isoefficacy hypothesis for UHDR and CONV treatment.

Normal skin damage/sparing.

The second primary goal of this study was to assess the relative skin effect of UHDR and CONV treatments at 1 × 25 and 1 × 30 Gy. Although irradiated skin effects presented in a number of morphological variations, we found categorizing the changes into two categories, dry desquamation and moist desquamation/ulceration was most helpful. While simple categorization may appear to lack dermatopathology specificity, especially in comparison to human and large animal situations, because mouse skin is very thin and lacks a superficial capillary/blood flow structure, it can undergo characteristic damage changes, i.e., moist desquamation to ulceration, very rapidly (24 h or less). Therefore, we found a simple damage criteria/grading system is most effective. Our data showed a statistically significant increase in the postirradiation time to moist desquamation/ulceration for UHDR treatment as compared to CONV treatment at 1 × 25 Gy. This difference, 7 days, translates to a 22% increase in the time to lesioning (sparing) after UHDR treatment. Gender was not a significant factor in the outcome. However, it should be noted that “time-to-lesioning” was modestly variable within individual groups. Our data did not a show time-to-lesioning (moist desquamation/ulceration) difference between UHDR and CONV treatments at 1 × 30 Gy. Gender was not a factor in the result. Although the prolongation of skin damage onset was longer for UHDR treated at 1 × 25 Gy, the overall incidence, type or degree of damage (histopathology assessment) was not different for UHDR or CONV treatments and after 25 or 30 Gy.

This study demonstrates the potential for reduced normal tissue damage after UHDR treatment, as compared to CONV treatment, at 1 × 25 Gy, but not at 1 × 30 Gy, suggesting a possible threshold for the FLASH effect at very high single doses. The study also supports the finding of many others that UHDR and CONV treatments have roughly isoeffective tumor control at modest doses and equal fractionate schemes. While our genetic and IHC data provides interesting and potentially useful preliminary data, especially about the expression of vascular and immune pathways, and the suggestion that UHDR irradiation results in a greater genetic expression variation than CONV irradiation, additional analysis of the bioinformatic data is necessary to provide a more comprehensive understanding of the role of individual genes. Finally, it is important to recognize that these studies were performed with UHDR beam structure of approximately 1 Gy/pulse and that new UHDR

irradiation information suggest higher doses per pulse may be important in the generation of an optimal FLASH effect.

ACKNOWLEDGMENTS

This research was supported by the Dartmouth Cancer Center CCSG: 5P30CA023108–37(Irradiation and Imaging Shared Resource, Genetic Shared Resource, Pathology Shared Resource). NIH/NCI grant: U01CA260446. Dartmouth Radiation Oncology Research Fund.

REFERENCES

1. Oweida A, Phan A, Vancourt B, Robin T, Hararah MK, Bhatia S, et al. Hypofractionated Radiotherapy Is Superior to Conventional Fractionation in an Orthotopic Model of Anaplastic Thyroid Cancer. Thyroid. 2018 Jun; 28(6):739–47. [PubMed: 29774792]
2. Ko EC, Forsythe K, Buckstein M, Kao J, Rosenstein BS. Radiobiological rationale and clinical implications of hypofractionated radiation therapy. Cancer/Radiothérapie. 2011 Jun; 15(3):221–9. [PubMed: 21514198]
3. Whelan TJ, Pignol JP, Levine MN, Julian JA, MacKenzie R, Parpia S, et al. Long-Term Results of Hypofractionated Radiation Therapy for Breast Cancer. N Engl J Med. 2010 Feb 11; 362(6):513–20. [PubMed: 20147717]
4. Favaudon V, Caplier L, Monceau V, Pouzoulet F, Sayarath M, Fouillade C, et al. Ultrahigh dose-rate FLASH irradiation increases the differential response between normal and tumor tissue in mice. Sci Transl Med [Internet]. 2014 Jul 16 [cited 2023 Feb 24]; 6(245). Available from: 10.1126/scitranslmed.3008973
5. Field SB, Bewley DK. Effects of Dose-rate on the Radiation Response of Rat Skin. Int J Radiat Biol Relat Stud Phys Chem Med. 1974 Jan; 26(3):259–67. [PubMed: 4547756]
6. Inada T, Nishio H, Amino S, Abe K, Saito K. High Dose-rate Dependence of Early Skin Reaction in Mouse. Int J Radiat Biol Relat Stud Phys Chem Med. 1980 Jan; 38(2):139–45. [PubMed: 6968733]
7. Hendry JH, Moore JV, Hodgson BW, Keene JP. The Constant Low Oxygen Concentration in All the Target Cells for Mouse Tail Radionecrosis. Radiat Res. 1982 Oct; 92(1):172. [PubMed: 7134382]
8. Böhlen TT, Germond JF, Petersson K, Ozsahin EM, Herrera FG, Bailat C, et al. Effect of conventional and ultra-high dose rate "FLASH" irradiations on preclinical tumour models: A systematic analysis. Int J Radiat Oncol. 2023 Jun; S0360301623005357.
9. Liljedahl E, Konradsson E, Gustafsson E, Jonsson KF, Olofsson JK, Ceberg C, et al. Long-term anti-tumor effects following both conventional radiotherapy and FLASH in fully immunocompetent animals with glioblastoma. Sci Rep. 2022 Jul 19; 12(1):12285. [PubMed: 35853933]
10. Soto LA, Casey KM, Wang J, Blaney A, Manjappa R, Breitkreutz D, et al. FLASH Irradiation Results in Reduced Severe Skin Toxicity Compared to Conventional-Dose-Rate Irradiation. Radiat Res. 2020; 194:618–24. [PubMed: 32853385]
11. Miles D, Sforza D, Wong JW, Siddiqui I, Tran PT, Rezaee M. FLASH Effects Induced by kV X-Rays in a Murine Skin Model. Int J Radiat Oncol. 2022 Nov; 114(3):e508.
12. Cunningham S, McCauley S, Vairamani K, Speth J, Girdhani S, Abel E, et al. FLASH Proton Pencil Beam Scanning Irradiation Minimizes Radiation-Induced Leg Contracture and Skin Toxicity in Mice. Cancers. 2021 Mar 1; 13(5):1012. [PubMed: 33804336]
13. Vozenin MC, De Fornel P, Petersson K, Favaudon V, Jaccard M, Germond JF, et al. The Advantage of FLASH Radiotherapy Confirmed in Mini-pig and Cat-cancer Patients. Clin Cancer Res. 2019 Jan 1; 25(1):35–42. [PubMed: 29875213]
14. Alaghband Y, Cheeks SN, Allen BD, Montay-Gruel P, Doan NL, Petit B, et al. Neuroprotection of Radiosensitive Juvenile Mice by Ultra-High Dose Rate FLASH Irradiation. Cancers. 2020 Jun 24; 12(6):1671. [PubMed: 32599789]
15. Simmons DA, Lartey FM, Schüler E, Rafat M, King G, Kim A, et al. Reduced cognitive deficits after FLASH irradiation of whole mouse brain are associated with less hippocampal dendritic spine loss and neuroinflammation. Radiother Oncol. 2019 Oct; 139:4–10. [PubMed: 31253467]

16. Jin JY, Gu A, Wang W, Oleinick NL, Machtay M, Kong FM. FLASH Dose Rate Effect on Circulating Immune Cells: A Potential Mechanism for FLASH-RT? Int J Radiat Oncol. 2020 Nov; 108(3):S7.
17. Dische S, Warburton MF, Jones D, Lartigau E. The recording of morbidity related to radiotherapy. Radiother Oncol. 1989 Oct; 16(2):103–8. [PubMed: 2595009]
18. Archambeau JO, Pezner R, Wasserman T. Pathophysiology of irradiated skin and breast. Int J Radiat Oncol. 1995 Mar; 31(5): 1171–85.
19. Hau E, Browne LH, Khanna S, Cail S, Cert G, Chin Y, et al. Radiotherapy Breast Boost with Reduced Whole-Breast Dose Is Associated With Improved Cosmesis: The Results of a Comprehensive Assessment From the St. George and Wollongong Randomized Breast Boost Trial. Int J Radiat Oncol. 2012 Feb; 82(2):682–9.
20. Krishnan L, Stanton AL, Collins CA, Liston VE, Jewell WR. Form or function? Part 2. Objective cosmetic and functional correlates of quality of life in women treated with breast-conserving surgical procedures and radiotherapy. Cancer. 2001 Jun 15; 91(12):2282–7. [PubMed: 11413516]
21. Rahman M, Ashraf MR, Zhang R, Bruza P, Dexter CA, Thompson L, et al. Electron FLASH Delivery at Treatment Room Isocenter for Efficient Reversible Conversion of a Clinical LINAC. Int J Radiat Oncol. 2021 Jul; 110(3):872–82.
22. Rückert M Immunological basis of abscopal antitumor responses induced by combination of distinct radiotherapy fractionation schedules with autologous tumor vaccines and checkpoint inhibition [Internet]. [Erlangen, Germany]: Friedrich-Alexander-Universität; 2021. Available from: https://opus4.kobv.de/opus4-fau/files/14865/Dissertation_Michael_Rueckert.pdf
23. Perkins JR, Dawes JM, McMahon SB, Bennett DL, Orengo C, Kohl M. ReadqPCR and NormqPCR: R packages for the reading, quality checking and normalisation of RT-qPCR quantification cycle (Cq) data. BMC Genomics. 2012; 13(1):296. [PubMed: 22748112]
24. Rahnenfuhrer AJ topGO: Enrichment Analysis for Gene Ontology. 2019. (https://bioconductor.org/packages/release/bioc/html/topGO.html)
25. Mitchell AL, Attwood TK, Babbitt PC, Blum M, Bork P, Bridge A, et al. InterPro in 2019: improving coverage, classification and access to protein sequence annotations. Nucleic Acids Res. 2019 Jan 8; 47(D1):D351–60. [PubMed: 30398656]
26. Geer LY, Marchler-Bauer A, Geer RC, Han L, He J, He S, et al. The NCBI BioSystems database. Nucleic Acids Res. 2010 Jan; 38(suppl_1):D492–6. [PubMed: 19854944]
27. Subramanian A, Tamayo P, Mootha VK, Mukherjee S, Ebert BL, Gillette MA, et al. Gene set enrichment analysis: A knowledge-based approach for interpreting genome-wide expression profiles. Proc Natl Acad Sci. 2005 Oct 25; 102(43):15545–50. [PubMed: 16199517]
28. Liberzon A, Subramanian A, Pinchback R, Thorvaldsdóttir H, Tamayo P, Mesirov JP. Molecular signatures database (MSigDB) 3.0. Bioinformatics. 2011 Jun 15; 27(12):1739–40. [PubMed: 21546393]
29. Fabregat A, Jupe S, Matthews L, Sidiropoulos K, Gillespie M, Garapati P, et al. The Reactome Pathway Knowledgebase. Nucleic Acids Res. 2018 Jan 4; 46(D1):D649–55. [PubMed: 29145629]
30. Slenter DN, Kutmon M, Hanspers K, Riutta A, Windsor J, Nunes N, et al. WikiPathways: a multifaceted pathway database bridging metabolomics to other omics research. Nucleic Acids Res. 2018 Jan 4; 46(D1):D661–7. [PubMed: 29136241]

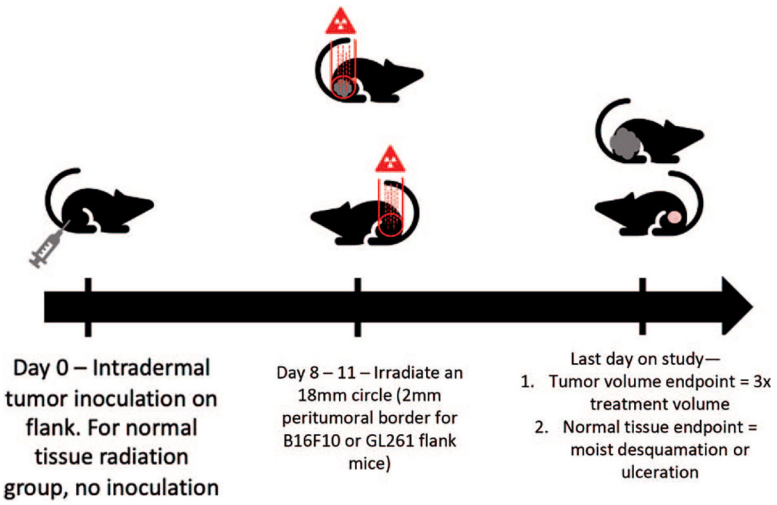

FIG. 1.

Experimental plan. Day 0 was the point of tumor inoculation, day 8 or 11 was the point of irradiation (depending on tumor type). Tumor-inoculated mice were removed from study either when the tumor reached 3 the irradiated volume, or when skin damage (dry/moist desquamation) was observed. B16F10 tumors irradiated for genetic or IHC analysis were assessed 96 hours postirradiation.

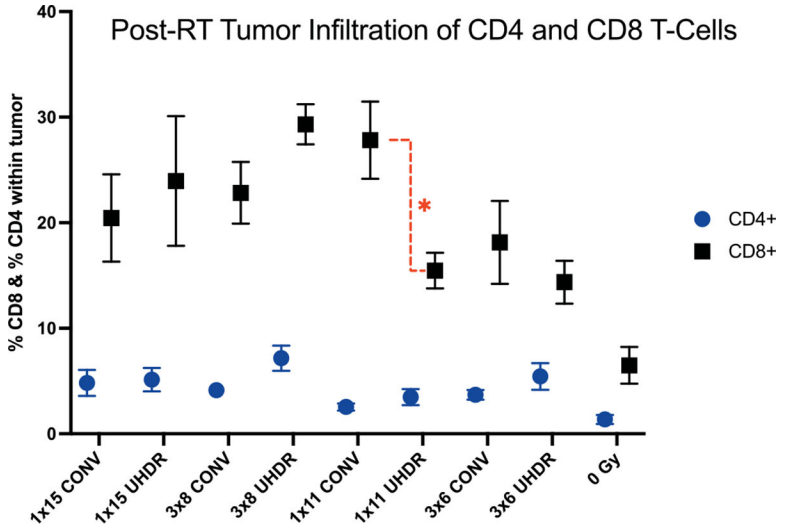

FIG. 2.

The above IHC figure demonstrates CD8 staining in a B16F10 mouse melanoma 96 h after various UHDR and CONV doses, with error bars indicating SEM. Histomorphometry of CD81 and CD41 cells in histologic sections demonstrated no significant difference in the tumor infiltration of CD4 cells after a range of radiation doses and fraction schemes for both UHDR and CONV irradiations. Only the 1 3 11 Gy dose group showed a statistical difference in CD81 cells between UHDR and CONV irradiations, with CONV treatment demonstrating a higher CD81 infiltration. There was not a corresponding difference in tumor control (tripling time) at 1 3 11 Gy. n ¼ 5 for each group. *P, 0.05 (t-test).

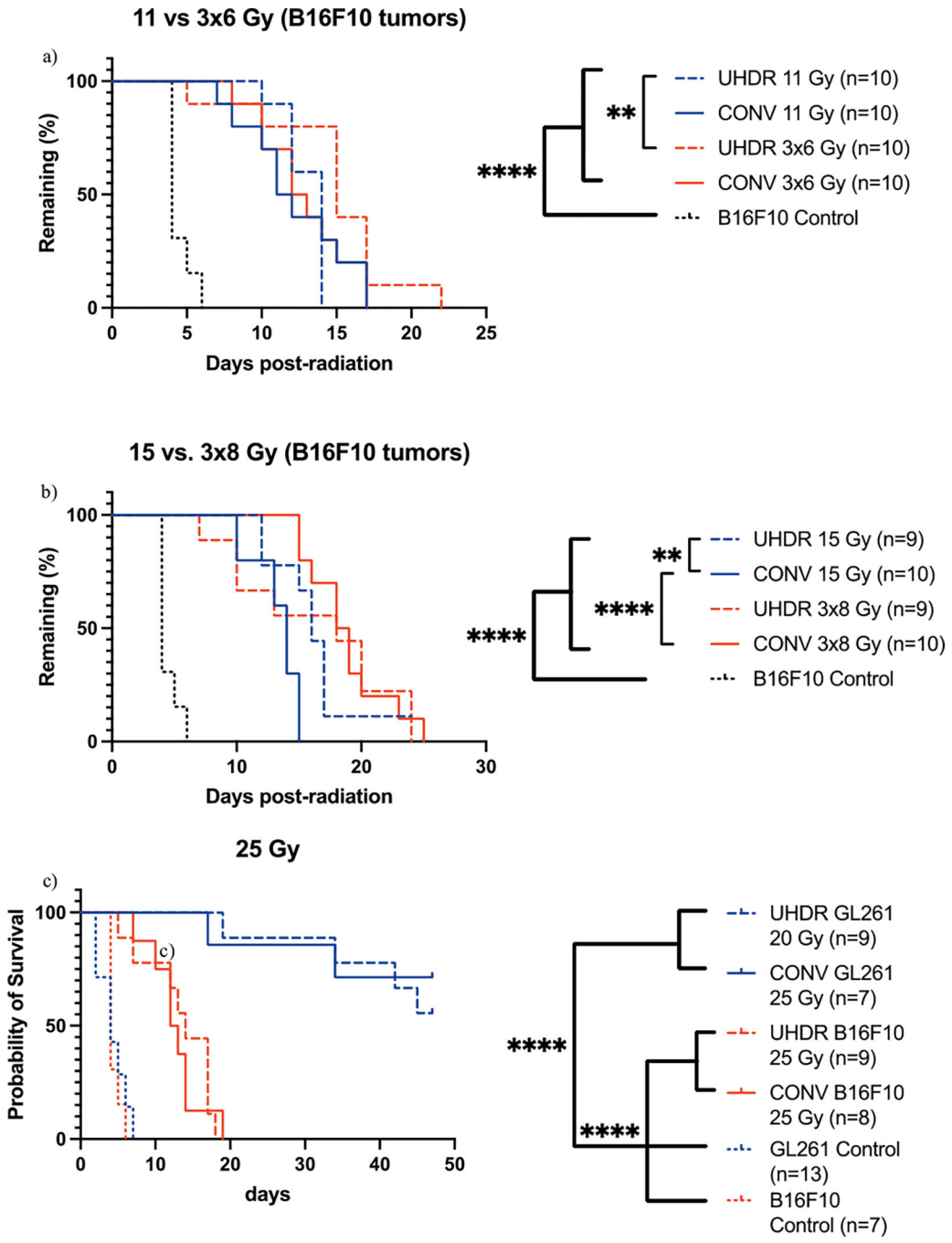

FIG. 3.

These Kaplan-Meier curves demonstrate the days after treatment required to reach a threefold increase in tumor volume for different UHDR and CONV fractionation schemes. The tumor tripling time for irradiated tumors was significantly different from nonirradiated tumors for all doses and dose rate (UHDR or CONV). (a) A significant difference in B16F10 tumor growth response ($P < 0.01$) was seen between 1×11 Gy and 3×6 Gy UHDR doses, but not between equivalent doses of UHDR and CONV. (b) Curve demonstrates a small but significant difference in B16F10 tumor growth response ($P < 0.01$) between UHDR and

CONV dose at 15 Gy and between 15 Gy and 3 × 8 Gy CONV doses. (c) At 1 × 20 Gy there was no difference in tumor tripling time, for either tumor type, after UHDR or CONV treatments ($P < 0.05$). *$P < 0.05$ (log-rank); **$P < 0.01$; ****$P < 0.0001$.

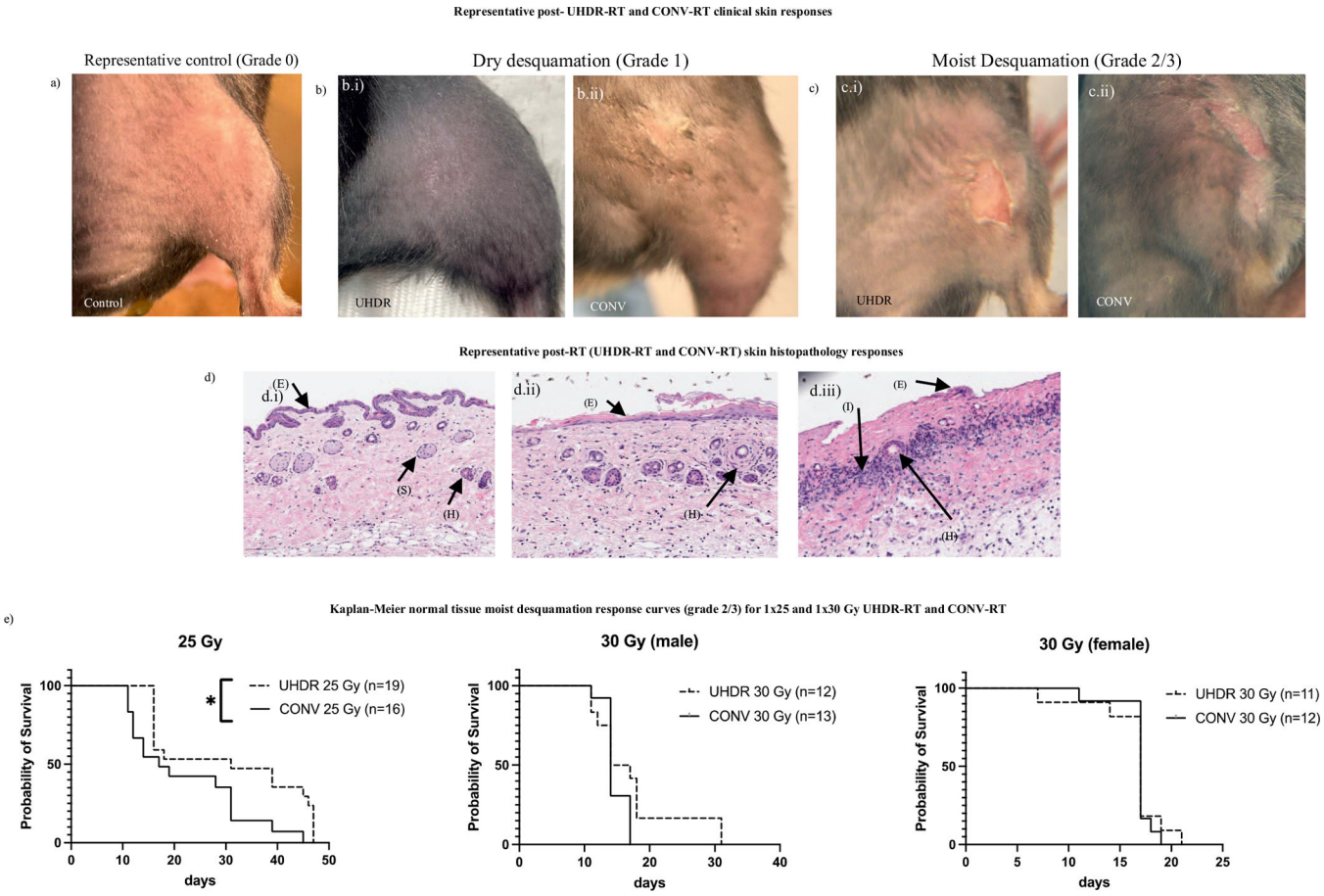

FIG. 4.

This figure demonstrates normal mouse skin, clinical postirradiation dermatopathology changes, histopathology validation of these changes (H&E staining) and Kaplan-Meier curves that quantify the times of lesioning differences between UHDR and CONV at 25 Gy and 30 Gy doses. Panels a-c demonstrate shaved normal mouse skin (4a), dry desquamation for UHDR and CONV doses (4b.i-ii, 25 Gy) and moist desquamation/ulceration (4c.i-ii, 25 Gy), although we determined the moist desquamation/ulceration endpoint (grade 2/3) to be the most accurate and useful in this situation, we believe it is important to demonstrate the full range of post-irradiation changes we observed. Normal mouse skin (4a,4d.i, grade 0) has a relative even layer of epidermis (E, arrow), minimal keratin and an average thickness of 3–4 epidermal cells. Histopathologically, normal mouse skin (4d, 10× magnification) has an even epidermal layer (E, arrow), uniform distribution of hair follicles (H, arrow) and sebaceous glands (S, arrow). There is an obvious paucity of superficial dermal capillaries, a unique characteristic of mouse skin. Dry desquamation: postirradiation dry desquamation (4bi.dii, grade 1) demonstrates skin wrinkling, unevenness and/or flaking. Histopathologically, dry desquamation changes (4dii, 10× magnification) included thinning and loss of epidermal integrity (E, arrow), ballooning of epidermal cells, loss of cell-to-cell contact, an increase in keratin, reduction in sebaceous glands (S, arrow) and hair follicles (F, arrow) and an increase in the density of dermal collagen. Moist desquamation: Postirradiation moist desquamation/ulceration (4c.i-ii, grade 2/3) demonstrates complete or

near-complete loss of the epidermis (dermis is clinically observable) often with the presence of superficial serum-like exudate. Histopathological analysis (4d.iii, 10× magnification) of moist desquamation/ulceration demonstrates loss of the epidermis (E, arrow), significant loss of adnexa structures including fibrosis encircling hair follicles (H, arrow), increased density of dermal collagen and, often infiltration of inflammatory cells (I, arrow). The Kaplan-Meier curves in 4e demonstrate a longer postirradiation latent period (time to lesioning) period for moist desquamation onset after UHDR treatment at 1 × 25 Gy, however there was no significant difference in the post-irradiation time to moist desquamation (UHDR vs. CONV) at 1 × 30 Gy. Both situations were statistically significant at $P < 0.05$.

TABLE 1

Beam Parameters for Tumor Radiation Treatment Methods

Parameter	CONV	UHDR
Beam energy	9 MeV	10 MeV
Circular cutout	ϕ = 18 mm	ϕ = 18 mm
Applicator size	6 × 6 cm	6 × 6 cm
SSD	100 cm[a]	100 cm[a]
Pulse repetition frequency	180 Hz	360 Hz
Dose per pulse (DPP)	0.0004744 Gy	0.72 Gy
Dose rate	0.1220 Gy/s	270 Gy/s

[a]Distance from source to surface of skin.

TABLE 2

Treatment Groups for Tumor Control Radiation Study

Radiation	Tumor	Prescribed dose (Gy)	BED (Gy)	Tumor control cohort (n)	IHC/genetic analysis cohort (n)
UHDR	B16F10	1 × 11	23.10	10	9
		1 × 15	37.50	9	9
		1 × 25	87.50	9	–
		3 × 6	28.80	10	9
		3 × 8	43.20	9	9
CONV	B16F10	1 × 11	23.10	10	9
		1 × 15	37.50	10	9
		1 × 25	87.50	8	–
		3 × 6	28.80	10	9
		3 × 8	43.20	10	9
UHDR	GL261	1 × 25	87.50	9	–
CONV	GL261	1 × 25	87.50	7	–

TABLE 3

Treatment Groups for Irradiated Normal Tissue Mouse Flank Skin

Radiation	Dose (Gy)	n
UHDR	1 × 25	19
CONV	1 × 25	16
UHDR	1 × 30	22
CONV	1 × 30	24

TABLE 4

Scoring System for Normal Skin Endpoint

Numerical score	Gross observation
0	Pre-treatment, normal: Gross: Normal, shaved, B6 mouse skin is slightly variable in color from grey to dark brown to light brown. Histopathologically mouse skin typically has a 3-cell-thick epidermal layer with minimal keratin. The dermis contains scattered hair follicles and sebaceous glands with uniformly stained collagen. There is a notable lack of superficial capillaries (neurovascular bundles) in the superficial mouse dermis.
1	Dry /pre-moist desquamation: Gross: Dry/pre-moist desquamation is characterized by variable skin wrinkling, erythema, pale coloration and/or flaking of the epidermal cells. Hair loss, even in shaved areas, can be observed. The lesion is not moist (meaning some level of epidermal integrity is maintained). Histopathologically, radiation-induced dry /pre-moist desquamation is characterized by thinning and denaturation of majority of the epidermal cells (complete loss of the epidermis in focal areas). Sebaceous glands have been lost and there is a notable reduction in the size, morphology and spacing of the hair follicles (smaller with peri-follicle fibrosis). As noted in Figure b.iii there may be scattered mononuclear inflammation.
2/3	Partial/full thickness epidermal lysis (ulceration)/desquamation with moisture: Gross: This lesion is typically characterized by partial or complete loss of the epidermis often with distinct visible edge boundaries between viable and lost epidermis. The lesion is often moist with an occasional serosanguinous fluid coating. Histopathologically, the lesion is characterized by loss of the epidermis often with denatured superficial dermis. There is general loss of adnexal structures and often notable inflammation between viable and non-viable dermis.

TABLE 5

Undirected GSA Scores for Each Pathway in Each Dose Group (Ranked), with Arrows Indicating Direction of Change (UHDR vs. CONV radiation treatment)

11 Gy	15 Gy	3 × 6 Gy	3 × 8 Gy
Mast-cell functions (1.94, ↓)	TLR (3.17, ↑)	TLR (2.21, ↓)	MHC (2.61, ↓)
NK-cell functions (1.84, ↓)	Dendritic-cell functions (2.94, ↓)	Mast cell functions (1.9, ↑)	Antigen processing (2.49, ↓)
Basic cell functions (1.81, ↑)	Antigen processing (2.64, ↓)	Macrophage functions (1.83, ↑)	NK-cell functions (2.36, ↓)
Adhesion (1.76, ↑)	TNF superfamily (2.48, ↓)	Adhesion (1.72, ↑)	T-Cell Functions (1.89, ↓)
Humoral (1.75, ↓)	Pathogen response (2.48, ↓)	Complement pathway (1.68, ↑)	Interferon (1.84, ↓)
Cell cycle (1.68, ↓)	Innate (2.47, ↓)	Cell cycle (1.64, ↓)	CD molecules (1.75, ↓)
Transporter functions (1.68, ↓)	Inflammation (2.44, ↓)	Transporter functions (1.63, ↑)	Interleukins (1.73, ↓)
T-cell functions (1.65, ↓)	T-cell functions (2.4, ↓)	CD molecules (1.48, ↑)	Adaptive (1.69, ↓)
Apoptosis (1.61, ↑)	Cancer progression (2.39, ↓)	Cancer progression (1.47, ↑)	TNF superfamily (1.66, ↓)
Leukocyte functions (1.6, ↑)	Apoptosis (2.37, ↑)	Pathogen response (1.46, ↑)	Cytokines and receptors (1.65, ↓)
Cancer progression (1.6, ↑)	Adhesion (2.33, ↑)	Apoptosis (1.44, ↑)	TLR (1.64, ↓)
CD molecules (1.58, ↓)	MHC (2.31, ↓)	Senescence (1.4, ↑)	Humoral (1.6, ↓)
Senescence (1.55, ↓)	Macrophage functions (2.29, ↓)	Basic cell functions (1.4, ↑)	Inflammation (1.59, ↓)
Complement pathway (1.48, ↓)	Chemokines and receptors (2.27, ↓)	Innate (1.37, ↑)	Apoptosis (1.54, ↓)
B-cell functions (1.47, ↓)	Transporter functions (2.27, ↓)	Interleukins (1.36, ↑)	B-cell functions (1.53, ↓)
Innate (1.47, ↑)	Leukocyte functions (2.26, ↓)	Cytokines and receptors (1.36, ↑)	Adhesion (1.51, ↑)
Macrophage functions (1.44, ↑)	Cytokines and receptors (2.25, ↓)	T-cell functions (1.35, ↑)	Innate (1.5, ↓)
Cytokines and receptors (1.42, ↓)	Adaptive (2.25, ↓)	Interferon (1.34, ↑)	Complement pathway (1.49, ↓)
Adaptive (1.4, ↓)	Interferon (2.25, ↓)	Humoral (1.34, ↑)	Cancer progression (1.49, ↓)
Chemokines and receptors (1.38, ↓)	Interleukins (2.22, ↓)	Inflammation (1.32, ↑)	Microglial functions (1.48, ↓)
TNF superfamily (1.35, ↑)	Humoral (2.2, ↓)	NK cell functions (1.32, ↑)	Leukocyte functions (1.43, ↑)
Inflammation (1.31, ↓)	B-cell functions (2.19, ↓)	Chemokines and receptors (1.31, ↑)	Basic cell functions (1.41, ↑)
Interferon (1.31, ↑)	CD molecules (2.18, ↓)	Dendritic cell functions (1.3, ↑)	Cell cycle (1.4, ↑)
Interleukins (1.31, ↓)	Complement pathway (2.15, ↓)	Leukocyte functions (1.28, ↑)	Chemokines and receptors (1.38, ↓)
Dendritic-cell functions (1.27, ↓)	NK-cell functions (2.13, ↓)	Antigen processing (1.26, ↑)	Transporter functions (1.38, ↓)
Pathogen response (1.27, ↑)	Basic cell functions (2.09, ↑)	MHC (1.25, ↑)	Mast-cell functions (1.27, ↓)
MHC (1.26, ↑)	Microglial functions (2.06, ↓)	B-cell functions (1.24, ↑)	Macrophage functions (1.23, ↓)

11 Gy	15 Gy	3 × 6 Gy	3 × 8 Gy
TLR (1.15, ↑)	Senescence (1.97, ↓)	Adaptive (1.23, ↑)	Pathogen response (1.15, ↑)
Antigen processing (1.04, ↑)	Cell cycle (1.7, ↑)	TNF superfamily (1.23, ↑)	Senescence (1.14, ↑)
Microglial functions (0.71, ↑)	Mast-cell functions (1.61, ↓)	Microglial functions (0.89, ↑)	Dendritic-cell functions (0.89, ↓)

Notes. Pathway-level expression data are shown for UHDR vs. CONV treatments across the 28 tested pathways. Pathways are arranged in order of high-to-low indirect global significance score (GSA) which is noted next to the pathway name. A higher indirect GSA corresponds to higher difference in expression of the given pathway for UHDR compared to CONV treatment. The direction of the difference is indicated by the arrow next to the GSA score; an upward arrow corresponds to higher expression in UHDR and vice versa. For example, at 11 Gy, the mast-cell function was the pathway that was expressed most differently in UHDR vs. CONV treatments, with expression being lower in the UHDR group as noted by the downward arrow.

TABLE 6

Radiation Type/Dose, Tumor Type, Days on Study

Radiation	Tumor	Dose (Gy)	Tumor tripling time (days)
UHDR	B16	1 × 11	13 ± 0.44
CONV	B16	1 × 11	12.2 ± 1.10
UHDR	B16	1 × 15	16.2 ± 1.18
CONV	B16	1 × 15	13.3 ± 0.60
UHDR	B16	1 × 25	13.3 ± 0.51[a]
CONV	B16	1 × 25	12.6 ± 0.43[a]
UHDR	B16	3 × 6	14.8 ± 0.95
CONV	B16	3 × 6	12.8 ± 0.95
UHDR	B16	3 × 8	16.2 ± 2.13
CONV	B16	3 × 8	18.8 ± 1.03
UHDR	GL261	1 × 25	41.7 ± 1.06
CONV	GL261	1 × 25	40.9 ± 1.65

[a]Animal tumors in the 1 × 25 Gy cohort were irradiated at comparatively higher tumor volumes than the tumors receiving other dose regimens. This situation did not change the relative tumor response outcome.

TABLE 7

Average Postirradiation Time Moist Desquamation Endpoint (error shown as SEM)

Mean days on study			
Dose (Gy)	**CONV**	**UHDR**	**P value**
1 × 25	21.13 ± 2.82	28.95 ± 3.28	0.0201
1 × 30 (male)	14.69 ± 0.45	17.42 ± 1.98	>0.05
1 × 30 (female)	16.75 ± 0.55	16.36 ± 1.61	>0.05